Sheng *et al. EURASIP Journal on Wireless Communications and Networking* (2017) 2017:48
DOI 10.1186/s13638-017-0831-5

EURASIP Journal on Wireless Communications and Networking

RESEARCH Open Access

Energy-efficient precoding in multicell networks with full-duplex base stations

Zhichao Sheng[1,2], Hoang Duong Tuan[2], Ho Huu Minh Tam[2], Ha H. Nguyen[3*] and Yong Fang[1]

Abstract

This paper considers multi-input multi-output (MIMO) multicell networks, where the base stations (BSs) are full-duplex transceivers, while uplink and downlink users are equipped with multiple antennas and operate in a half-duplex mode. The problem of interest is to design linear precoders for BSs and users to optimize the network's energy efficiency. Given that the energy efficiency objective is not a ratio of concave and convex functions, the commonly used Dinkelbach-type algorithms are not applicable. We develop a low-complexity path-following algorithm that only invokes one simple convex quadratic program at each iteration, which converges at least to the local optimum. Numerical results demonstrate the performance advantage of our proposed algorithm in terms of energy efficiency.

Keywords: Energy efficiency, Cooperative multicell network, Full-duplexing transceiver, Precoder design, Path-following convex quadratic programming

1 Introduction

Energy saving has become a pressing ecological/economical concern in dealing with global warming. From this perspective, it is important to reduce the amount of carbon emissions associated with operating modern and sophisticated communication networks [1, 2]. Energy saving also helps to reduce the operational cost since energy consumption constitutes a significant portion of the network expenditure. Green cellular networks (see, e.g., [3, 4]), which aim at optimizing energy efficiency (EE) for communications in terms of bits per joule per hertz have drawn considerable research interests in recent years (see, e.g., [5–8] and the references therein). In fact, EE has been recognized as the new figure-of-merit in assessing the quality and efficiency of future communication networks and beyond (see, e.g., [9–11]). For multicell networks, EE requires new approaches for interference management as compared to the more traditional performance metrics [12–17], which mainly aim at maximizing the spectral efficiency (SE) in terms of bits per second per hertz.

Full-duplex (FD) communication, which allows simultaneous transmission and reception (over the same frequency band) to and from multiple downlink users (DLUs) and multiple uplink users (ULUs), respectively, has emerged as one of the key techniques for the fifth-generation (5G) networks [18–23]. Nevertheless, a challenging issue in realizing FD communication is that the interference is very severe, not only because of the residual FD self-interference (SI) but also the cross interference between the uplink and the downlink transmissions. In this paper, we consider the design of linear precoders to optimize energy efficiency under quality-of-service (QoS) constraints in FD multi-input multi-output (MIMO) multicell networks. Specifically, the BSs are equipped with multiple antennas and operate in the FD mode. There are two separate groups of multi-antenna users (UEs) in each cell, the ULUs and the DLUs, and both groups operate in the hall-duple (HD) mode. To the authors' best knowledge, such precoder design problem has not been thoroughly addressed, even for MIMO cooperative multicell networks with half-duplex base stations.

It is pointed out that, since the rate function of the users is nonconcave, the QoS in terms of user's minimum rate constitutes difficult nonconvex constraints, which are addressed very recently in [24] in a different optimization problem. On the other hand, the EE objective is not a ratio of concave and convex functions in order to facilitate the

*Correspondence: ha.nguyen@usask.ca
[3]Department of Electrical and Computer Engineering, University of Saskatchewan, Saskatoon, Canada
Full list of author information is available at the end of the article

Dinkelbach-type algorithm [25], which is the main tool for obtaining computational solutions of EE optimization problems (see, e.g. [26–28] and the references therein). To get around such nonconvexity issue, references [29] and [30] consider the specific zero-forcing precoders to completely cancel the interferences so that the user's rate function becomes concave and the QoS constraints become convex, while the EE objective becomes a ratio of concave and convex functions. This then allows the application of the Dinkelbach-type algorithm. It should be noted, however, that although having the convex QoS constraints on zero-forcing precoders, the EE optimization problems are still very difficult and there are no polynomial-time algorithms available to solve them. Furthermore, EE optimization for zero-forcing precoders only applies to the case that the number of antennas at each BS is much larger than the total number of users' antennas. As for the FD cooperative multicell networks considered in this paper, the interference cannot be completely canceled out due to the presence of self-interference [19, 21, 22]; hence, the Dinkelbach-type algorithm is not applicable.

Motivated from the above observations, the aim of this paper is to develop a novel solution approach that directly tackles the nonconvexity of the concerned EE optimization problem. The proposed algorithm is a path-following computational procedure, which invokes a simple convex quadratic program at each iteration. The rest of the paper is structured as follows. Section 2 provides the problem formulation. Section 3 develops its computational solution. Section 4 is devoted to numerical examples. Section 5 concludes the paper.

Notation. All variables are denoted by mathematical sans serif letters. Vectors and matrices are boldfaced. $\mathbf{I}_n$ denotes the identity matrix of size $n \times n$, while $\mathbf{1}_{n\times m}$ is the all-one matrix of size $n \times m$. The notation $(\cdot)^H$ stands for the Hermitian transpose, $|\mathbf{A}|$ denotes the determinant of a square matrix $\mathbf{A}$, and Trace($\mathbf{A}$) denotes the trace of a matrix $\mathbf{A}$. The inner product $\langle \mathbf{X}, \mathbf{Y}\rangle$ is defined as Trace($\mathbf{X}^H\mathbf{Y}$), and therefore, the Frobenius squared norm of a matrix $\mathbf{X}$ is $||\mathbf{X}||^2 = \text{Trace}(\mathbf{X}\mathbf{X}^H)$. The notation $\mathbf{A} \succeq \mathbf{B}$ ($\mathbf{A} \succ \mathbf{B}$, respectively) means that $\mathbf{A} - \mathbf{B}$ is a positive semidefinite (definite, respectively) matrix. $\mathbb{E}[\cdot]$ denotes the expectation operator and $\Re\{\cdot\}$ denotes the real part of a complex number.

2 System model and optimization problem formulations

We consider an MIMO cooperative network consisting of I cells. As illustrated in Fig. 1, the BS of cell $i \in \{1, \ldots, I\}$ serves a group of D DLUs in the downlink (DL) channel and a group of U ULUs in the uplink (UL) channel. Each BS operates in the FD mode and is equipped with $N \triangleq N_1 + N_2$ antennas, where N_1 antennas are used to transmit and the remaining N_2 antennas to receive signals. In cell i, DLU (i, j_{D}) and ULU (i, j_{U}) operate in the HD mode and each is equipped with N_r antennas. Similar to other works on precoding and interference suppression (see, e.g., [6, 12, 13, 15–17, 29] and references therein), it is assumed in this paper that there are high-performance channel estimation mechanisms in place and a central processing unit is available to collect and disseminate the relevant CSI.

In the DL, a complex-valued vector $\mathbf{s}_{i,j_{\mathsf{D}}} \in \mathbb{C}^{d_1}$ is the symbols intended for DLU (i, j_{D}), where $\mathbb{E}\left[\mathbf{s}_{i,j_{\mathsf{D}}}(\mathbf{s}_{i,j_{\mathsf{D}}})^H\right] = \mathbf{I}_{d_1}$, d_1 is the number of concurrent data streams, and $d_1 \le \min\{N_1, N_r\}$. Denote by $\mathsf{V}_{i,j_{\mathsf{D}}} \in \mathbb{C}^{N_1\times d_1}$ the complex-valued precoding matrix for DLU (i, j_{D}) . Similarly, in the UL, $\mathbf{s}_{i,j_{\mathsf{U}}} \in \mathbb{C}^{d_2}$ is the symbols sent by ULU (i, j_{U}), where $\mathbb{E}\left[\mathbf{s}_{i,j_{\mathsf{U}}}(\mathbf{s}_{i,j_{\mathsf{U}}})^H\right] = \mathbf{I}_{d_2}$, d_2 is the number of concurrent data streams, and $d_2 \le \min\{N_2, N_r\}$. The precoding matrix of ULU (i, j_{U}) is denoted as $\mathsf{V}_{i,j_{\mathsf{U}}} \in \mathbb{C}^{N_r\times d_2}$. Define

$$\begin{aligned} &\mathcal{I} \triangleq \{1, 2, \ldots, I\}; \quad \mathcal{D} \triangleq \{1_{\mathsf{D}}, 2_{\mathsf{D}}, \ldots, D_{\mathsf{D}}\};\\ &\mathcal{U} \triangleq \{1_{\mathsf{U}}, 2_{\mathsf{U}}, \ldots, U_{\mathsf{U}}\}; \quad \mathcal{S}_1 \triangleq \mathcal{I} \times \mathcal{D}; \quad \mathcal{S}_2 \triangleq \mathcal{I} \times \mathcal{U};\\ &\mathsf{V} \triangleq [\mathsf{V}_{i,j}]_{(i,j)\in\mathcal{S}_1\cup\mathcal{S}_2}. \end{aligned} \tag{1}$$

In the DL channel, the received signal at DLU (i, j_{D}) is expressed as:

$$\begin{aligned} y_{i,j_{\mathsf{D}}} \triangleq\ & \underbrace{\mathbf{H}_{i,i,j_{\mathsf{D}}}\mathsf{V}_{i,j_{\mathsf{D}}}\mathbf{s}_{i,j_{\mathsf{D}}}}_{\text{desired signal}} + \underbrace{\sum_{(m,\ell_{\mathsf{D}})\in\mathcal{S}_1\setminus(i,j_{\mathsf{D}})} \mathbf{H}_{m,i,j_{\mathsf{D}}}\mathsf{V}_{m,\ell_{\mathsf{D}}}\mathbf{s}_{m,\ell_{\mathsf{D}}}}_{\text{DL interference}}\\ &+ \underbrace{\sum_{\ell_{\mathsf{U}}\in\mathcal{U}} \mathbf{H}_{i,j_{\mathsf{D}},\ell_{\mathsf{U}}}\mathsf{V}_{i,\ell_{\mathsf{U}}}\mathbf{s}_{i,\ell_{\mathsf{U}}}}_{\text{ULintracell interference}} + \mathbf{n}_{i,j_{\mathsf{D}}}, \end{aligned} \tag{2}$$

where $\mathbf{H}_{m,i,j_{\mathsf{D}}} \in \mathbb{C}^{N_r\times N_1}$ and $\mathbf{H}_{i,j_{\mathsf{D}},\ell_{\mathsf{U}}} \in \mathbb{C}^{N_r\times N_r}$ are the channel matrices from BS m to DLU (i, j_{D}) and from ULU (i, ℓ_{U}) to DLU (i, j_{D}), respectively. Also, $\mathbf{n}_{i,j_{\mathsf{D}}}$ is the additive white Gaussian noise (AWGN) sample, modeled as circularly symmetric complex Gaussian random variable with variance σ_{D}^2. Suppose that each BS i employs dirty-paper coding (DPC)-based transmission strategy (see, e.g., [31]) in broadcasting signals to its users. Then the corresponding DL throughput for user (i, j_{D}) is [32, eq. (4)]

$$f_{i,j_{\mathsf{D}}}(\mathsf{V}) \triangleq \ln\left|\mathbf{I}_{N_r} + \mathcal{L}_{i,j_{\mathsf{D}}}(\mathsf{V}_{i,j_{\mathsf{D}}})\mathcal{L}_{i,j_{\mathsf{D}}}^H(\mathsf{V}_{i,j_{\mathsf{D}}})\Psi_{i,j_{\mathsf{D}}}^{-1}(\mathsf{V})\right|, \tag{3}$$

where $\mathcal{L}_{i,j_{\mathsf{D}}}(\mathsf{V}_{i,j_{\mathsf{D}}}) \triangleq \mathbf{H}_{i,i,j_{\mathsf{D}}}\mathsf{V}_{i,j_{\mathsf{D}}}$ and

$$\mathcal{L}_{i,j_{\mathsf{D}}}(\mathsf{V}_{i,j_{\mathsf{D}}})\mathcal{L}_{i,j_{\mathsf{D}}}^H(\mathsf{V}_{i,j_{\mathsf{D}}}) = \mathbf{H}_{i,i,j_{\mathsf{D}}}\mathsf{V}_{i,j_{\mathsf{D}}}\mathsf{V}_{i,j_{\mathsf{D}}}^H\mathbf{H}_{i,i,j_{\mathsf{D}}}^H, \tag{4}$$

$$\begin{aligned} \Psi_{i,j_{\mathsf{D}}}(\mathsf{V}) \triangleq\ & \sum_{(m,\ell_{\mathsf{D}})\in\mathcal{S}_1\setminus\{(i,\ell_{\mathsf{D}}),\ell=j,\ldots,D\}} \mathbf{H}_{m,i,j_{\mathsf{D}}}\mathsf{V}_{m,\ell_{\mathsf{D}}}\mathsf{V}_{m,\ell_{\mathsf{D}}}^H\mathbf{H}_{m,i,j_{\mathsf{D}}}^H\\ &+ \sum_{\ell_{\mathsf{U}}\in\mathcal{U}} \mathbf{H}_{i,j_{\mathsf{D}},\ell_{\mathsf{U}}}\mathsf{V}_{i,\ell_{\mathsf{U}}}\mathsf{V}_{i,\ell_{\mathsf{U}}}^H\mathbf{H}_{i,j_{\mathsf{D}},\ell_{\mathsf{U}}}^H + \sigma_{\mathsf{D}}^2\mathbf{I}_{N_r}. \end{aligned} \tag{5}$$

Note that DPC-based broadcasting is a capacity achieving transmission, which enables user (i, j_{D}) view the term

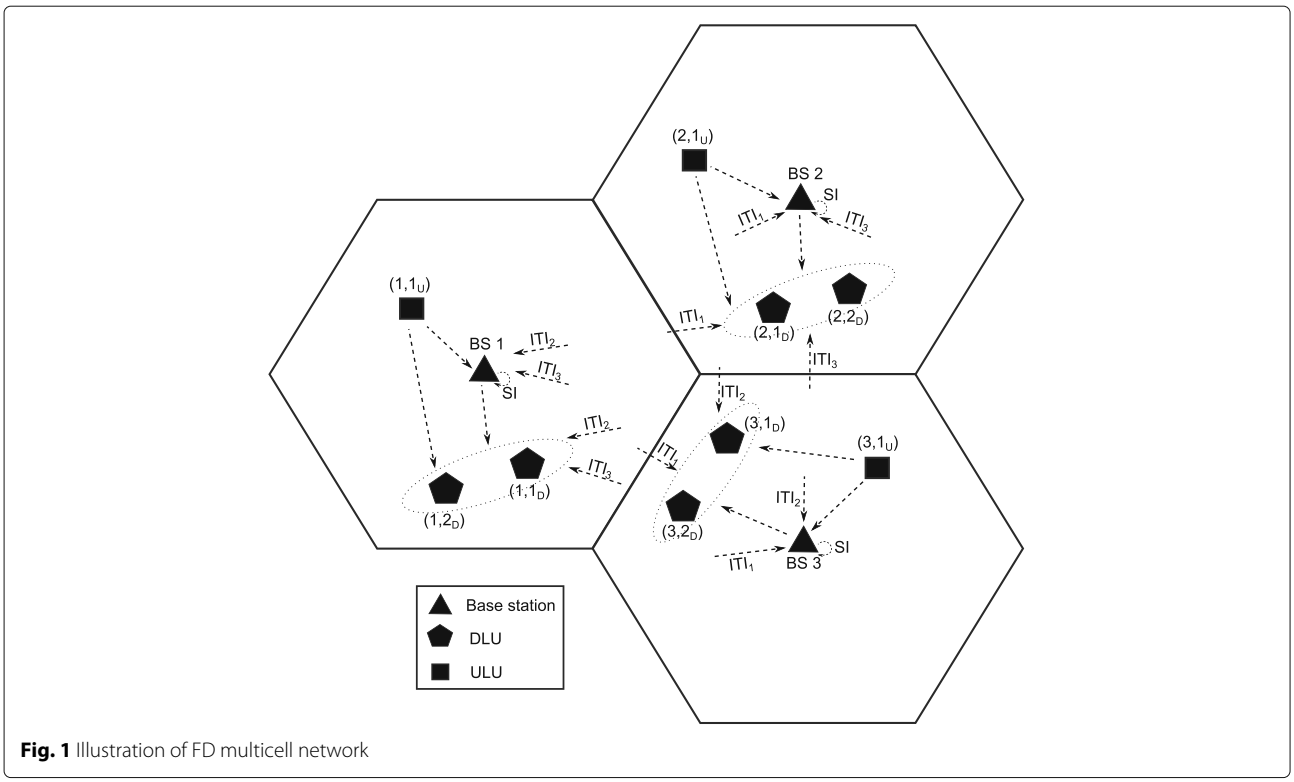

Fig. 1 Illustration of FD multicell network

$\sum_{k_{\mathsf{D}}<j_{\mathsf{D}}} \mathbf{H}_{i,i,j_{\mathsf{D}}} \mathsf{V}_{i,k_{\mathsf{D}}} \mathbf{s}_{i,k_{\mathsf{D}}}$ as known non-causally and thus reduces it from the interference in (3) [33, Lemma 1]. This term is still present under conventional broadcast, for which the interference mapping $\Psi_{i,j_{\mathsf{D}}}(\mathsf{V})$ in (3) becomes

$$\Psi_{i,j_{\mathsf{D}}}(\mathsf{V}) \triangleq \sum_{(m,\ell_{\mathsf{D}})\in\mathcal{S}_1\setminus\{(i,j_{\mathsf{D}})\}} \mathbf{H}_{m,i,j_{\mathsf{D}}} \mathsf{V}_{m,\ell_{\mathsf{D}}} \mathsf{V}_{m,\ell_{\mathsf{D}}}^H \mathbf{H}_{m,i,j_{\mathsf{D}}}^H + \sum_{\ell_{\mathsf{U}}\in\mathcal{U}} \mathbf{H}_{i,j_{\mathsf{D}},\ell_{\mathsf{U}}} \mathsf{V}_{i,\ell_{\mathsf{U}}} \mathsf{V}_{i,\ell_{\mathsf{U}}}^H \mathbf{H}_{i,j_{\mathsf{D}},\ell_{\mathsf{U}}}^H + \sigma_{\mathsf{D}}^2 \mathbf{I}_{N_r}. \quad (6)$$

It is pointed out that our below development is still applicable to the case of conventional broadcast.

In the UL channel, the received signal at BS i can be expressed as

$$y_i \triangleq \underbrace{\sum_{\ell_{\mathsf{U}}\in\mathcal{U}} \mathbf{H}_{i,\ell_{\mathsf{U}},i} \mathsf{V}_{i,\ell_{\mathsf{U}}} \mathbf{s}_{i,\ell_{\mathsf{U}}}}_{\text{desired signal}} + \underbrace{\sum_{m\in\mathcal{I}\setminus\{i\}} \sum_{\ell_{\mathsf{U}}\in\mathcal{U}} \mathbf{H}_{m,\ell_{\mathsf{U}},i} \mathsf{V}_{m,\ell_{\mathsf{U}}} \mathbf{s}_{m,\ell_{\mathsf{U}}}}_{\text{UL interference}} + \underbrace{\mathbf{H}_i^{\mathcal{SI}} \sum_{\ell_{\mathsf{D}}\in\mathcal{D}} \mathsf{V}_{i,\ell_{\mathsf{D}}} \tilde{\mathbf{s}}_{i,\ell_{\mathsf{D}}}}_{\text{residual SI}} + \underbrace{\sum_{m\in\mathcal{I}\setminus\{i\}} \mathbf{H}_{m,i}^{\mathcal{B}} \sum_{j_{\mathsf{D}}\in\mathcal{D}} \mathsf{V}_{m,j_{\mathsf{D}}} \mathbf{s}_{m,\mathbf{s}_{\mathsf{D}}}}_{\text{DLintercell interference}} + \mathbf{n}_i, \quad (7)$$

where $\mathbf{H}_{m,\ell_{\mathsf{U}},i} \in \mathbb{C}^{N_2\times N_r}$ and $\mathbf{H}_{m,i}^{\mathcal{B}} \in \mathbb{C}^{N_2\times N_1}$ are the channel matrices from ULU (m,ℓ_{U}) to BS i and from BS m to BS i, respectively. The channel matrix $\mathbf{H}_i^{\mathcal{SI}} \in \mathbb{C}^{N_2\times N_1}$ represents the residual self-loop channel from the transmit antennas to the receive antennas at BS i after all real-time interference cancelations in both analog and digital domains [22, 34] are accounted for (more detailed discussion on modelling the SI channel can be found in [22, 34]). The additive Gaussian noise vector $\tilde{\mathbf{s}}_{i,\ell_{\mathsf{D}}}$ with $\mathbb{E}\left[\tilde{\mathbf{s}}_{i,j_{\mathsf{D}}}(\tilde{\mathbf{s}}_{i,j_{\mathsf{D}}})^H\right] = \sigma_{\mathsf{SI}}^2 \mathbf{I}_{d_1}$ models the effects of the analog circuit's non-ideality and the limited dynamic range of the analog-to-digital converter (ADC) [19, 23, 34, 35]. The SI level σ_{SI}^2 is the ratio of the average SI powers before and after the SI cancelation process. Lastly, $\mathbf{n}_i$ is the AWGN sample, modeled as circularly-symmetric complex Gaussian random variable with variance σ_{U}^2.

By treating the entries of the self-loop channel $\mathbf{H}_i^{\mathcal{SI}}$ in (7) as independent circularly symmetric complex Gaussian random variables with zero mean and unit variance, the power of the residual SI in (7) is

$$\sigma_{\mathsf{SI}}^2 \mathbb{E}\left\{\mathbf{H}_i^{\mathcal{SI}} \left(\sum_{\ell_D\in\mathsf{D}} \mathsf{V}_{i,\ell_D} \mathsf{V}_{i,\ell_D}^H\right) (\mathbf{H}_i^{\mathcal{SI}})^H\right\} = \sigma_{\mathsf{SI}}^2 \left(\sum_{\ell_D\in\mathsf{D}} ||\mathsf{V}_{i,\ell_D}||^2\right) \mathbf{I}_{N_r}. \quad (8)$$

It is important to point out that the above power expression only depends on the BS transmit power, and it cannot be changed by precoder matrices $\mathsf{V}_{i,\ell_{\mathsf{D}}}$.

Given that the minimum mean square error–successive interference cancelation (MMSE-SIC) detector is the most popular detection method in uplink communications, this type of receiver is also adopted in this paper. Under the

MMSE-SIC receiver, the achievable uplink throughput at BS i is given as [36]

$$f_i(\mathsf{V}) \triangleq \ln \left| \mathbf{I}_{N_2} + \mathcal{L}_i(\mathsf{V}_{\mathsf{U}i}) \mathcal{L}_i^H(\mathsf{V}_{\mathsf{U}i}) \Psi_i^{-1}(\mathsf{V}) \right|, \tag{9}$$

where

$$\begin{aligned} \mathsf{V}_{\mathsf{U}i} &\triangleq (\mathsf{V}_{i,\ell_{\mathsf{U}}})_{\ell_{\mathsf{U}} \in \mathcal{U}}, \mathcal{L}_i(\mathsf{V}_{\mathsf{U}i}) \\ &\triangleq \left[\mathbf{H}_{i,1_{\mathsf{U}},i} \mathsf{V}_{i,1_{\mathsf{U}}}, \mathbf{H}_{i,2_{\mathsf{U}},i} \mathsf{V}_{i,2_{\mathsf{U}}}, \ldots, \mathbf{H}_{i,U_{\mathsf{U}},i} \mathsf{V}_{i,U_{\mathsf{U}}} \right], \end{aligned} \tag{10}$$

and

$$\mathcal{L}_i(\mathsf{V}_{\mathsf{U}i}) \mathcal{L}_i^H(\mathsf{V}_{\mathsf{U}i}) = \sum_{\ell=1}^{U} \mathbf{H}_{i,\ell_{\mathsf{U}},i} \mathsf{V}_{i,\ell_{\mathsf{U}}} \mathsf{V}_{i,\ell_{\mathsf{U}}}^H \mathbf{H}_{i,\ell_{\mathsf{U}},i}^H, \tag{11}$$

$$\begin{aligned} \Psi_i(\mathsf{V}) \triangleq & \sum_{m \in I \setminus \{i\}} \sum_{\ell_{\mathsf{U}} \in \mathcal{U}} \mathbf{H}_{m,\ell_{\mathsf{U}},i} \mathsf{V}_{m,\ell_{\mathsf{U}}} \mathsf{V}_{m,\ell_{\mathsf{U}}}^H \mathbf{H}_{m,\ell_{\mathsf{U}},i}^H \\ & + \sigma_{\mathrm{SI}}^2 \Big(\sum_{\ell_D \in \mathsf{D}} ||\mathsf{V}_{i,\ell_D}||^2 \Big) \mathbf{I}_{N_r} \\ & + \sum_{m \in \mathcal{I} \setminus \{i\}} \mathbf{H}_{m,i}^{\mathcal{B}} \left(\sum_{j_{\mathsf{D}} \in \mathcal{D}} \mathsf{V}_{m,j_{\mathsf{D}}} \mathsf{V}_{m,j_{\mathsf{D}}}^H \right) (\mathbf{H}_{m,i}^{\mathcal{B}})^H + \sigma_{\mathsf{U}}^2 \mathbf{I}_{N_2}. \end{aligned} \tag{12}$$

Following [37], the consumed power P_i^{tot} of cell i can be modeled as

$$P_i^{\mathrm{tot}}(\mathsf{V}) = \zeta P_i^t(\mathsf{V}) + P^{\mathrm{BS}} + UP^{\mathrm{UE}}, \tag{13}$$

where $P_i^t(\mathsf{V}) \triangleq \sum_{j_{\mathsf{D}} \in \mathcal{D}} ||\mathsf{V}_{i,j_{\mathsf{D}}}||^2 + \sum_{j_{\mathsf{U}} \in \mathcal{U}} ||\mathsf{V}_{i,j_{\mathsf{U}}}||^2$ is the total transmit power of BS and UEs in cell i and ζ is the reciprocal of drain efficiency of power amplifier. Alo $P^{\mathrm{BS}} = N_1 P_b$ and $P^{\mathrm{UE}} = N_r P_u$ are the circuit powers of BS and UE, respectively, where P_b and P_u represent the per-antenna circuit power of BS and UEs, respectively. Consequently, the energy efficiency of cell i is defined by

$$\frac{\sum_{j_{\mathsf{D}} \in \mathcal{D}} f_{i,j_{\mathsf{D}}}(\mathsf{V}) + f_i(\mathsf{V})}{P_i^{\mathrm{tot}}(\mathsf{V})}. \tag{14}$$

In this paper, we consider the following precoder design to optimize the network's energy efficiency:

$$\max_{\mathsf{V}} \min_{i \in \mathcal{I}} \frac{\sum_{j_{\mathsf{D}} \in \mathcal{D}} f_{i,j_{\mathsf{D}}}(\mathsf{V}) + f_i(\mathsf{V})}{P_i^{\mathrm{tot}}(\mathsf{V})} \text{ s.t.} \tag{15a}$$

$$\sum_{j_{\mathsf{D}} \in \mathcal{D}} ||\mathsf{V}_{i,j_{\mathsf{D}}}||^2 \le P_{\mathrm{BS}}^{\max},\ i \in \mathcal{I}, \tag{15b}$$

$$||\mathsf{V}_{i,j_{\mathsf{U}}}||^2 \le P_{\mathrm{UE}}^{\max},\ (i,j_{\mathsf{U}}) \in \mathcal{S}_2, \tag{15c}$$

$$f_{i,j_{\mathsf{D}}}(\mathsf{V}) \ge r_{i,j_{\mathsf{D}}}^{\min},\ (i,j_{\mathsf{D}}) \in \mathcal{S}_1 \tag{15d}$$

$$f_i(\mathsf{V}) \ge r_i^{\mathsf{U},\min},\ i \in \mathcal{I}, \tag{15e}$$

where (15b)-(15c) limit the transmit powers for each BS and ULU, while (15d)-(15e) are the QoS constraints for both downlink and uplink transmissions.

On the other hand, the problem of optimizing the energy efficiency in *DL transmission only* is formulated as follows:

$$\max_{\mathsf{V}^{\mathrm{DL}}=[\mathsf{V}_{i,j_{\mathsf{D}}}]_{(i,j_{\mathsf{D}}) \in \mathcal{S}_1}} \min_{i \in \mathcal{I}} \frac{\sum_{j_{\mathsf{D}} \in \mathcal{D}} f_{i,j_{\mathsf{D}}}^{\mathrm{DL}}(\mathsf{V}^{\mathrm{DL}})}{\zeta \sum_{j_{\mathsf{D}} \in \mathcal{D}} ||\mathsf{V}_{i,j_{\mathsf{D}}}||^2 + P^{\mathrm{BS}}} \text{ s.t. } (15b), \tag{16a}$$

$$f_{i,j_{\mathsf{D}}}^{\mathrm{DL}}(\mathsf{V}^{\mathrm{DL}}) \ge r_{i,j_{\mathsf{D}}}^{\min},\ (i,j_{\mathsf{D}}) \in \mathcal{S}_1 \tag{16b}$$

with

$$\begin{aligned} f_{i,j_{\mathsf{D}}}^{\mathrm{DL}}(\mathsf{V}^{\mathrm{DL}}) \triangleq & \ln \Big| \mathbf{I}_{N_r} + \mathbf{H}_{i,i,j_{\mathsf{D}}} \mathsf{V}_{i,j_{\mathsf{D}}} \mathsf{V}_{i,j_{\mathsf{D}}}^H \mathbf{H}_{i,i,j_{\mathsf{D}}}^H \\ & \times \Big(\sum_{(m,\ell_{\mathsf{D}}) \in \mathcal{S}_1 \setminus \{(i,\ell_{\mathsf{D}}), \ell=j,\ldots,D\}} \mathbf{H}_{m,i,j_{\mathsf{D}}} \mathsf{V}_{m,\ell_{\mathsf{D}}} \\ & \times \mathsf{V}_{m,\ell_{\mathsf{D}}}^H \mathbf{H}_{m,i,j_{\mathsf{D}}}^H + \sigma_{\mathsf{D}}^2 \mathbf{I}_{N_r} \Big)^{-1} \Big|. \end{aligned} \tag{17}$$

Likewise, the problem of optimizing the energy efficiency in the *UL transmission only* is

$$\max_{\mathsf{V}^{\mathrm{UL}}=[\mathsf{V}_{i,\ell_{\mathsf{U}}}]_{(i,\ell_{\mathsf{U}}) \in \mathcal{S}_2}} \min_{i \in \mathcal{I}} \frac{f_i^{\mathrm{UL}}(\mathsf{V}^{\mathrm{UL}})}{\zeta \sum_{\ell_{\mathsf{U}} \in \mathcal{U}} ||\mathsf{V}_{i,\ell_{\mathsf{U}}}||^2 + UP^{\mathrm{UE}}} \text{ s.t. } (15c), \tag{18a}$$

$$f_i^{\mathrm{UL}}(\mathsf{V}^{\mathrm{UL}}) \ge r_i^{\mathsf{U},\min},\ i \in \mathcal{I}, \tag{18b}$$

with

$$\begin{aligned} f_i^{\mathrm{UL}}(\mathsf{V}^{\mathrm{UL}}) \triangleq \ln \Big| & \mathbf{I}_{N_2} + \sum_{\ell=1}^{U} \mathbf{H}_{i,\ell_{\mathsf{U}},i} \mathsf{V}_{i,\ell_{\mathsf{U}}} \mathsf{V}_{i,\ell_{\mathsf{U}}}^H \mathbf{H}_{i,\ell_{\mathsf{U}},i}^H \\ & \times \left(\sum_{m \in \mathcal{I} \setminus \{i\}} \sum_{\ell_{\mathsf{U}} \in \mathcal{U}} \mathbf{H}_{m,\ell_{\mathsf{U}},i} \mathsf{V}_{m,\ell_{\mathsf{U}}} \mathsf{V}_{m,\ell_{\mathsf{U}}}^H \mathbf{H}_{m,\ell_{\mathsf{U}},i}^H + \sigma_{\mathsf{U}}^2 \mathbf{I}_{N_2} \right)^{-1} \Big|. \end{aligned} \tag{19}$$

As discussed before, for the downlink EE optimization problem (16), references [29] and [30] apply zero-forcing precoders so that all the interference terms in (5) are completely canceled, making $f_{i,j_{\mathsf{D}}}^{\mathrm{DL}}(\mathsf{V}^{\mathrm{DL}}) = \ln \left| \mathbf{I}_{N_r} + \mathbf{H}_{i,i,j_{\mathsf{D}}} \mathsf{V}_{i,j_{\mathsf{D}}} \mathsf{V}_{i,j_{\mathsf{D}}}^H \mathbf{H}_{i,i,j_{\mathsf{D}}}^H / \sigma_{\mathsf{D}}^2 \right|$. Then by making the

variable change $\mathsf{X}_{i,j_\mathsf{D}} = \mathsf{V}_{i,j_\mathsf{D}}\mathsf{V}_{i,j_\mathsf{D}}^H$, the EE optimization for zero-forcing precoders becomes:

$$\max_{\mathsf{X}^{\mathrm{DL}}=[\mathsf{X}_{i,j_\mathsf{D}}]_{(i,j_\mathsf{D})\in\mathcal{S}_1}} \min_{i\in\mathcal{I}} \times \frac{\sum_{j_\mathsf{D}\in\mathcal{D}} \ln\left|\mathbf{I}_{N_r} + \mathbf{H}_{i,i,j_\mathsf{D}}\mathsf{X}_{i,j_\mathsf{D}}^H\mathbf{H}_{i,i,j_\mathsf{D}}^H/\sigma_\mathsf{D}^2\right|}{\zeta\sum_{j_\mathsf{D}\in\mathcal{D}}\mathrm{Trace}(\mathsf{X}_{i,j_\mathsf{D}}) + P^{\mathrm{BS}}} \quad \text{s.t.} \tag{20a}$$

$$\sum_{j_\mathsf{D}\in\mathcal{D}}\mathrm{Trace}(\mathsf{X}_{i,j_\mathsf{D}}) \le P_{\mathrm{BS}}^{\max},\ i\in\mathcal{I}, \tag{20b}$$

$$\ln\left|\mathbf{I}_{N_r} + \mathbf{H}_{i,i,j_\mathsf{D}}\mathsf{X}_{i,j_\mathsf{D}}^H\mathbf{H}_{i,i,j_\mathsf{D}}^H/\sigma_\mathsf{D}^2\right| \ge r_{i,j_\mathsf{D}}^{\min},\ (i,j_\mathsf{D})\in\mathcal{S}_1, \tag{20c}$$

$$\mathsf{X}^{\mathrm{DL}} \in Z_{zf}, \tag{20d}$$

where the last linear constraint (20d) is to explicitly specify a zero-forcing precoder. Since the numerator in the objective (20a) is concave in $\mathsf{X}_{i,j_\mathsf{D}}$, the problem expressed in (20) is *maximin* optimization of concave-convex function ratios. To solve such problem, references [29] and [30] use the Dinkelbach-type algorithm [25]. Specifically, the optimal value of (20) is found as the maximum of γ for which the optimal value of the following convex program is nonnegative:

$$\max_{\mathsf{X}^{\mathrm{DL}}=[\mathsf{X}_{i,j_\mathsf{D}}]_{(i,j_\mathsf{D})\in\mathcal{S}_1}} \min_{i\in\mathcal{I}} \left[\sum_{j_\mathsf{D}\in\mathcal{D}} \ln\left|\mathbf{I}_{N_r} + \mathbf{H}_{i,i,j_\mathsf{D}}\mathsf{X}_{i,j_\mathsf{D}}^H\mathbf{H}_{i,i,j_\mathsf{D}}^H/\sigma_\mathsf{D}^2\right| - \gamma\left(\zeta\sum_{j_\mathsf{D}\in\mathcal{D}}\mathrm{Trace}(\mathsf{X}_{i,j_\mathsf{D}}) + P^{\mathrm{BS}}\right)\right] \quad \text{s.t.}\ (20b),(20c),(20d). \tag{21}$$

It should be noted that, although being convex for fixed γ, the program (21) is still computationally difficult. This is because the concave objective function and convex constraints (20c) in (21) involve log-det functions. In fact, no polynomial-time algorithms are known to find the solution. Another issue is that the zero-forcing constraint (20d) in (21) would rule out the effectiveness of the optimization, unless the total number $(N \cdot I)$ of the BSs' antennas is much larger than the total number $(I \cdot D \cdot N_r)$ of DLUs' antennas.

The optimal value of (7) is still the maximum of $\gamma > 0$ such that the optimal value of the following program is nonnegative

$$\max_{\mathsf{V}} \min_{i\in\mathcal{I}} \left[\sum_{j_\mathsf{D}\in\mathcal{D}} f_{i,j_\mathsf{D}}(\mathsf{V}) + f_i(\mathsf{V}) - \gamma P_i^{\mathrm{tot}}(\mathsf{V})\right] \quad \text{s.t.}\ (15b)-(15e). \tag{22}$$

However, problem (22) is a very difficult nonconvex optimization even for a fixed $\gamma > 0$ because its objective function is obviously nonconcave while its constraints (15e) are highly nonconvex. In fact, one can see that (22) for a fixed γ is not easier than the original nonconvex optimization problem (15). In the next section we will develop a path-following procedure for computing the solution of (15) that avoids the setting (22).

3 Path-following quadratic programming

With the newly introduced variable $t = (t_1, \ldots, t_I)$, $t_i > 0$, $i = 1, 2, \ldots, I$ and under the convex quadratic constraints

$$\zeta\sum_{j_\mathsf{D}\in\mathcal{D}}||\mathsf{V}_{i,j_\mathsf{D}}||^2 + \sum_{j_\mathsf{U}\in\mathcal{U}}||\mathsf{V}_{i,j_\mathsf{U}}||^2 + P^{\mathrm{BS}} + UP^{\mathrm{UE}} \le t_i, i\in\mathcal{I}, \tag{23}$$

problem (15) is equivalently expressed by

$$\max_{\mathsf{V},\mathsf{t}} \mathcal{P}(\mathsf{V},\mathsf{t}) \triangleq \min_{i\in\mathcal{I}} \frac{\sum_{j_\mathsf{D}\in\mathcal{D}} f_{i,j_\mathsf{D}}(\mathsf{V}) + f_i(\mathsf{V})}{\mathsf{t}_i} \quad \text{s.t.}\ (15b),(15c),(15d),(15e),(23). \tag{24}$$

Let

$$\begin{aligned}\mathcal{M}_{i,j_\mathsf{D}}(\mathsf{V}) &\triangleq \mathcal{L}_{i,j_\mathsf{D}}(\mathsf{V}_{i,j_\mathsf{D}})\mathcal{L}_{i,j_\mathsf{D}}^H(\mathsf{V}_{i,j_\mathsf{D}}) + \Psi_{i,j_\mathsf{D}}(\mathsf{V}) \\ &\succeq \Psi_{i,j_\mathsf{D}}(\mathsf{V}),\end{aligned} \tag{25}$$

and

$$\begin{aligned}\mathcal{M}_i(\mathsf{V}) &\triangleq \mathcal{L}_i(\mathsf{V}_{\mathsf{U}i})\mathcal{L}_i^H(\mathsf{V}_{\mathsf{U}i}) + \Psi(\mathsf{V}_i) \\ &\succeq \Psi(\mathsf{V}_i).\end{aligned} \tag{26}$$

At $\mathbf{V}^{(\kappa)} \triangleq \left[\mathbf{V}_{i,j}^{(\kappa)}\right]_{(i,j)\in\mathcal{S}_1\cup\mathcal{S}_2}$, which is feasible to (15b)-(15e), define the following quadratic functions in V:

$$\begin{aligned}\Theta_{i,j_\mathsf{D}}^{(\kappa)}(\mathsf{V}) &\triangleq a_{i,j_\mathsf{D}}^{(\kappa)} + 2\Re\left\{\langle\Psi_{i,j_\mathsf{D}}^{-1}(\mathbf{V}^{(\kappa)})\mathcal{L}_{i,j_\mathsf{D}}(\mathbf{V}_{i,j_\mathsf{D}}^{(\kappa)}), \mathcal{L}_{i,j_\mathsf{D}}(\mathsf{V}_{i,j_\mathsf{D}})\rangle\right\} \\ &\quad - \langle\Psi_{i,j_\mathsf{D}}^{-1}(\mathbf{V}^{(\kappa)}) - \mathcal{M}_{i,j_\mathsf{D}}^{-1}(\mathbf{V}^{(\kappa)}), \mathcal{M}_{i,j_\mathsf{D}}(\mathsf{V})\rangle \\ &= a_{i,j_\mathsf{D}}^{(\kappa)} + 2\Re\left\{\mathrm{Trace}\left((\mathbf{V}_{i,j_\mathsf{D}}^{(\kappa)})^H\mathbf{H}_{i,i,j_\mathsf{D}}^H\Psi_{i,j_\mathsf{D}}^{-1}(\mathbf{V}^{(\kappa)})\mathbf{H}_{i,i,j_\mathsf{D}}\mathsf{V}_{i,j_\mathsf{D}}\right)\right\} \\ &\quad - \sum_{(m,\ell_\mathsf{D})\in\mathcal{S}_1\setminus\{(i,\ell_\mathsf{D}),\ell=j+1,\ldots,D\}} \mathrm{Trace}\left(\mathsf{V}_{m,\ell_\mathsf{D}}^H\mathbf{H}_{m,i,j_\mathsf{D}}^H\left(\Psi_{i,j_\mathsf{D}}^{-1}(\mathbf{V}^{(\kappa)}) - \mathcal{M}_{i,j_\mathsf{D}}^{-1}(\mathbf{V}^{(\kappa)})\right)\mathbf{H}_{m,i,j_\mathsf{D}}\mathsf{V}_{m,\ell_\mathsf{D}}\right) \\ &\quad - \sum_{\ell_\mathsf{U}\in\mathcal{U}} \mathrm{Trace}\left(\mathsf{V}_{i,\ell_\mathsf{U}}^H\mathbf{H}_{i,j_\mathsf{D},\ell_\mathsf{U}}^H\left(\Psi_{i,j_\mathsf{D}}^{-1}(\mathbf{V}^{(\kappa)}) - \mathcal{M}_{i,j_\mathsf{D}}^{-1}(\mathbf{V}^{(\kappa)})\right)\mathbf{H}_{i,j_\mathsf{D},\ell_\mathsf{U}}\mathsf{V}_{i,\ell_\mathsf{U}}\right) \\ &\quad - \sigma_\mathsf{D}^2\mathrm{Trace}\left(\Psi_{i,j_\mathsf{D}}^{-1}(\mathbf{V}^{(\kappa)}) - \mathcal{M}_{i,j_\mathsf{D}}^{-1}(\mathbf{V}^{(\kappa)})\right)\end{aligned} \tag{27}$$

and

$$\begin{aligned}\Theta_i^{(\kappa)}(\mathsf{V}) \triangleq\ & a_i^{(\kappa)} + 2\Re\left\{\langle\Psi_i^{-1}(\mathbf{V}^{(\kappa)})\mathcal{L}_i(\mathbf{V}_{\mathsf{U}i}^{(\kappa)}), \mathcal{L}_i(\mathsf{V}_{\mathsf{U}i})\rangle\right\} \\ & - \langle\Psi_i^{-1}(\mathbf{V}^{(\kappa)}) - \mathcal{M}_i^{-1}(\mathbf{V}^{(\kappa)}), \mathcal{M}_i(\mathsf{V})\rangle \\ =\ & a_i^{(\kappa)} + 2\sum_{\ell=1}^{U}\Re\left\{\mathrm{Trace}\left((\mathbf{V}_{i,\ell_{\mathsf{U}}}^{(\kappa)})^H\mathbf{H}_{i,\ell_{\mathsf{U}},i}^H\Psi_i^{-1}(\mathbf{V}^{(\kappa)})\mathbf{H}_{i,\ell_{\mathsf{U}},i}\mathsf{V}_{i,\ell_{\mathsf{U}}}\right)\right\} \\ & - \sum_{m\in\mathcal{I}}\sum_{\ell_{\mathsf{U}}\in\mathcal{U}}\mathrm{Trace}\left(\mathsf{V}_{m,\ell_{\mathsf{U}}}^H\mathbf{H}_{m,\ell_{\mathsf{U}},i}^H(\Psi_i^{-1}(\mathbf{V}^{(\kappa)})\right. \\ & \left.-\mathcal{M}_i^{-1}(\mathbf{V}^{(\kappa)}))\mathbf{H}_{m,\ell_{\mathsf{U}},i}\mathsf{V}_{m,\ell_{\mathsf{U}}}\right) \\ & - \sigma_{\mathrm{SI}}^2\mathrm{Trace}(\left(\Psi_i^{-1}(\mathbf{V}^{(\kappa)}) - \mathcal{M}_i^{-1}(\mathbf{V}^{(\kappa)})\right)\sum_{\ell_{\mathsf{D}}\in\mathcal{D}}||\mathsf{V}_{i,\ell_{\mathsf{D}}}||^2 \\ & - \sum_{m\in\mathcal{I}\setminus\{i\}}\sum_{j_{\mathsf{D}}\in\mathcal{D}}\mathrm{Trace}\left(\mathsf{V}_{m,j_{\mathsf{D}}}^H(\mathbf{H}_{m,i}^{\mathcal{B}})^H(\Psi_i^{-1}(\mathbf{V}^{(\kappa)})\right. \\ & \left.-\mathcal{M}_i^{-1}(\mathbf{V}^{(\kappa)}))\mathbf{H}_{m,i}^{\mathcal{B}}\mathsf{V}_{m,j_{\mathsf{D}}}\right) \\ & - \sigma_{\mathsf{U}}^2\mathrm{Trace}\left(\Psi_i^{-1}(\mathbf{V}^{(\kappa)}) - \mathcal{M}_i^{-1}(\mathbf{V}^{(\kappa)})\right).\end{aligned} \tag{28}$$

These functions are concave because $\Psi_{i,j_{\mathsf{D}}}^{-1}(\mathbf{V}^{(\kappa)}) - \mathcal{M}_{i,j_{\mathsf{D}}}^{-1}(\mathbf{V}^{(\kappa)}) \succeq 0$ and $\Psi_i^{-1}(\mathbf{V}^{(\kappa)}) - \mathcal{M}_i^{-1}(\mathbf{V}^{(\kappa)}) \succeq 0$. Also

$$\begin{aligned}0 > a_{i,j_{\mathsf{D}}}^{(\kappa)} =& f_{i,j_{\mathsf{D}}}(\mathbf{V}^{(\kappa)}) - \langle\Psi_{i,j_{\mathsf{D}}}^{-1}(\mathbf{V}^{(\kappa)})\mathcal{L}_{i,j_{\mathsf{D}}}(\mathbf{V}_{i,j_{\mathsf{D}}}^{(\kappa)}), \mathcal{L}_{i,j_{\mathsf{D}}}(\mathbf{V}_{i,j_{\mathsf{D}}}^{(\kappa)})\rangle \\ 0 > a_i^{(\kappa)} =& f_i(\mathbf{V}^{(\kappa)}) - \langle\Psi_i^{-1}(\mathbf{V}^{(\kappa)})\mathcal{L}_i(\mathbf{V}_{\mathsf{U}i}^{(\kappa)}), \mathcal{L}_i(\mathbf{V}_{\mathsf{U}i}^{(\kappa)})\rangle,\end{aligned} \tag{29}$$

which follows from the inequality[1]

$$\ln|\mathbf{I}+\mathbf{X}| \le \mathrm{Trace}(\mathbf{X}), \quad \forall\,\mathbf{X}\succeq 0. \tag{30}$$

The following result shows that the highly nonlinear and nonconcave functions $f_{i,j_{\mathsf{D}}}(\cdot)$ and $f_i(\cdot)$ in problem (15) can be globally and locally approximated by concave quadratic functions.

Theorem 1 *It is true that* [24]

$$f_{i,j_{\mathsf{D}}}(\mathbf{V}^{(\kappa)}) = \Theta_{i,j_{\mathsf{D}}}^{(\kappa)}(\mathbf{V}^{(\kappa)}) \text{ and } f_{i,j_{\mathsf{D}}}(\mathsf{V}) \ge \Theta_{i,j_{\mathsf{D}}}^{(\kappa)}(\mathsf{V}) \quad \forall\,\mathsf{V}, \tag{31}$$

$$f_i(\mathbf{V}^{(\kappa)}) = \Theta_i^{(\kappa)}(\mathbf{V}^{(\kappa)}) \text{ and } f_i(\mathsf{V}) \ge \Theta_i^{(\kappa)}(\mathsf{V}) \quad \forall\,\mathsf{V}. \tag{32}$$

It follows from the above theorem that the nonconvex QoS constraints (15d) and (15e) can be innerly approximated by the following convex quadratic constraints:

$$\Theta_{i,j_{\mathsf{D}}}^{(\kappa)}(\mathsf{V}) \ge r_{i,j_{\mathsf{D}}}^{\min},\ (i,j_{\mathsf{D}})\in\mathcal{S}_1; \quad \Theta_i^{(\kappa)}(\mathsf{V}) \ge r_i^{\mathsf{U},\min},\ i\in\mathcal{I}. \tag{33}$$

These constraints also yield

$$\begin{aligned}&\Re\left\{\langle\Psi_{i,j_{\mathsf{D}}}^{-1}(\mathbf{V}^{(\kappa)})\mathcal{L}_{i,j_{\mathsf{D}}}(\mathbf{V}_{i,j_{\mathsf{D}}}^{(\kappa)}), \mathcal{L}_{i,j_{\mathsf{D}}}(\mathsf{V}_{i,j_{\mathsf{D}}})\rangle\right\} \ge \\ &-a_{i,j_{\mathsf{D}}}^{(\kappa)} + \langle\Psi_{i,j_{\mathsf{D}}}^{-1}(\mathbf{V}^{(\kappa)}) - \mathcal{M}_{i,j_{\mathsf{D}}}^{-1}(\mathbf{V}^{(\kappa)}), \mathcal{M}_{i,j_{\mathsf{D}}}(\mathsf{V})\rangle \ge 0,\ (i,j_{\mathsf{D}})\in\mathcal{S}_1,\end{aligned} \tag{34}$$

and

$$\begin{aligned}&\Re\left\{\langle\Psi_i^{-1}(\mathbf{V}^{(\kappa)})\mathcal{L}_i(\mathbf{V}_{\mathsf{U}i}^{(\kappa)}), \mathcal{L}_i(\mathsf{V}_{\mathsf{U}i})\rangle\right\} \ge \\ &-a_i^{(\kappa)} + \langle\Psi_i^{-1}(\mathbf{V}^{(\kappa)}) - \mathcal{M}_i^{-1}(\mathbf{V}^{(\kappa)}), \mathcal{M}_i(\mathsf{V})\rangle \ge \quad 0,\ i\in\mathcal{I}.\end{aligned} \tag{35}$$

Therefore, by using the inequality[2]

$$\frac{x}{t_i} \ge 2\frac{\sqrt{x^{(\kappa)}}\sqrt{x}}{t_i^{(\kappa)}} - \frac{x^{(\kappa)}}{(t_i^{(\kappa)})^2}t_i \quad \forall x>0, x^{(\kappa)}>0, t_i>0, t_i^{(\kappa)}>0, \tag{36}$$

we obtain

$$\begin{aligned}\frac{\Re\left\{\langle\Psi_{i,j_{\mathsf{D}}}^{-1}(\mathbf{V}^{(\kappa)})\mathcal{L}_{i,j_{\mathsf{D}}}(\mathbf{V}_{i,j_{\mathsf{D}}}^{(\kappa)}), \mathcal{L}_{i,j_{\mathsf{D}}}(\mathsf{V}_{i,j_{\mathsf{D}}})\rangle\right\}}{\mathsf{t}_i} &\ge \varphi_{i,j_{\mathsf{D}}}^{(\kappa)}(\mathsf{V}_{i,j_{\mathsf{D}}},\mathsf{t}_i), \\ \frac{\Re\left\{\langle\Psi_i^{-1}(\mathbf{V}^{(\kappa)})\mathcal{L}_i(\mathbf{V}_{\mathsf{U}i}^{(\kappa)}), \mathcal{L}_i(\mathsf{V}_{\mathsf{U}i})\rangle\right\}}{\mathsf{t}_i} &\ge \varphi_i^{(\kappa)}(\mathsf{V}_{\mathsf{U}i},\mathsf{t}_i)\end{aligned} \tag{37}$$

for

$$\begin{aligned}\varphi_{i,j_{\mathsf{D}}}^{(\kappa)}(\mathsf{V}_{i,j_{\mathsf{D}}},\mathsf{t}_i) &\triangleq 2b_{i,j_{\mathsf{D}}}^{(\kappa)}\sqrt{\Re\left\{\langle\Psi_{i,j_{\mathsf{D}}}^{-1}(\mathbf{V}^{(\kappa)})\mathcal{L}_{i,j_{\mathsf{D}}}(\mathbf{V}_{i,j_{\mathsf{D}}}^{(\kappa)}), \mathcal{L}_{i,j_{\mathsf{D}}}(\mathsf{V}_{i,j_{\mathsf{D}}})\rangle\right\}} - c_{i,j_{\mathsf{D}}}^{(\kappa)}\mathsf{t}_i \\ \varphi_i^{(\kappa)}(\mathsf{V}_{\mathsf{U}i},\mathsf{t}_i) &\triangleq 2b_i^{(\kappa)}\sqrt{\Re\left\{\langle\Psi_i^{-1}(\mathbf{V}^{(\kappa)})\mathcal{L}_i(\mathbf{V}_{\mathsf{U}i}^{(\kappa)}), \mathcal{L}_i(\mathsf{V}_{\mathsf{U}i})\rangle\right\}} - c_i^{(\kappa)}\mathsf{t}_i,\end{aligned} \tag{38}$$

where

$$\begin{aligned}b_{i,j_{\mathsf{D}}}^{(\kappa)} &= \frac{\sqrt{\langle\Psi_{i,j_{\mathsf{D}}}^{-1}\left(\mathbf{V}^{(\kappa)}\right)\mathcal{L}_{i,j_{\mathsf{D}}}\left(\mathbf{V}_{i,j_{\mathsf{D}}}^{(\kappa)}\right), \mathcal{L}_{i,j_{\mathsf{D}}}\left(\mathbf{V}_{i,j_{\mathsf{D}}}^{(\kappa)}\right)\rangle}}{\mathsf{t}_i^{(\kappa)}} \\ &> 0,\ c_{i,j_{\mathsf{D}}}^{(\kappa)} = \left(b_{i,j_{\mathsf{D}}}^{(\kappa)}\right)^2 > 0, \\ b_i^{(\kappa)} &= \frac{\sqrt{\Re\left\{\langle\Psi_i^{-1}\left(\mathbf{V}^{(\kappa)}\right)\mathcal{L}_i\left(\mathbf{V}_{\mathsf{U}i}^{(\kappa)}\right), \mathcal{L}_i\left(\mathbf{V}_{\mathsf{U}i}^{(\kappa)}\right)\rangle\right\}}}{\mathsf{t}_i^{(\kappa)}} \\ &> 0,\ c_i^{(\kappa)} = \left(b_i^{(\kappa)}\right)^2 > 0.\end{aligned} \tag{39}$$

It is pointed out that functions $\varphi_{i,j_{\mathsf{D}}}^{(\kappa)}$ and $\varphi_i^{(\kappa)}$ are concave [38]. Furthermore, define functions

$$\begin{aligned} g_{i,j_{\mathsf{D}}}^{(\kappa)}(\mathsf{V},\mathsf{t}_i) &\triangleq \frac{a_{i,j_{\mathsf{D}}}^{(\kappa)}}{\mathsf{t}_i} + 2\varphi_{i,j_{\mathsf{D}}}^{(\kappa)}(\mathsf{V}_{i,j_{\mathsf{D}}},\mathsf{t}_i) \\ &\quad - \frac{\langle \Psi_{i,j_{\mathsf{D}}}^{-1}(\mathbf{V}^{(\kappa)}) - \mathcal{M}_{i,j_{\mathsf{D}}}^{-1}(\mathbf{V}^{(\kappa)}), \mathcal{M}_{i,j_{\mathsf{D}}}(\mathsf{V})\rangle}{\mathsf{t}_i}, \\ g_i^{(\kappa)}(\mathsf{V},\mathsf{t}_i) &\triangleq \frac{a_i^{(\kappa)}}{\mathsf{t}_i} + 2\varphi_i^{(\kappa)}(\mathsf{V}_{\mathsf{U}i},\mathsf{t}_i) \\ &\quad - \frac{\langle \Psi_i^{-1}(\mathbf{V}^{(\kappa)}) - \mathcal{M}_i^{-1}(\mathbf{V}^{(\kappa)}), \mathcal{M}_i(\mathsf{V})\rangle}{\mathsf{t}_i}, \end{aligned} \tag{40}$$

which are concave. This can be justified by observing that the first terms of these two functions, $a_{i,j_{\mathsf{D}}}^{(\kappa)}/\mathsf{t}_i$ and $a_i^{(\kappa)}/\mathsf{t}_i$, are concave as $a_{i,j_{\mathsf{D}}}^{(\kappa)} < 0$ and $a_i^{(\kappa)} < 0$ by (29), while their second terms have been shown to be concave as above, and their third terms are concave according to [39].

We now address the nonconvex problem (15) by successively solving the following convex quadratic program (QP):

$$\begin{aligned} \max_{\mathsf{V},\mathsf{t}} \ & \mathcal{P}^{(\kappa)}(\mathsf{V},\mathsf{t}) \triangleq \min_{i\in\mathcal{I}} \left[\sum_{j_{\mathsf{D}}\in\mathcal{D}} g_{i,j_{\mathsf{D}}}^{(\kappa)}(\mathsf{V},\mathsf{t}_i) + g_i^{(\kappa)}(\mathsf{V},\mathsf{t}_i) \right] \\ \text{s.t.} \quad & (15b), (15c), (23), (33). \end{aligned} \tag{41}$$

Note that (41) involves $n = 2(N_1 \cdot d_1 \cdot I \cdot D + N_r \cdot d_2 \cdot I \cdot U) + I$ scalar real variables and $m = I \cdot D + 3 \cdot I + I \cdot U$ quadratic constraints so its computational complexity is $\mathcal{O}(n^2 m^{2.5} + m^{3.5})$.

Proposition 1 *Let* $(\mathbf{V}^{(\kappa)}, \mathbf{t}^{(\kappa)})$ *be a feasible point to (24). The optimal solution* $(\mathbf{V}^{(\kappa+1)}, \mathbf{t}^{(\kappa+1)})$ *of convex program (41) is feasible to the nonconvex program (24) and it is better than* $(\mathbf{V}^{(\kappa)}, \mathbf{t}^{(\kappa)})$*, i.e.,*

$$\mathcal{P}(\mathbf{V}^{(\kappa+1)}, \mathbf{t}^{(\kappa)}) \geq \mathcal{P}(\mathbf{V}^{(\kappa)}, \mathbf{t}^{(\kappa)}). \tag{42}$$

as long as $(\mathbf{V}^{(\kappa+1)}, \mathbf{t}^{(\kappa+1)}) \neq (\mathbf{V}^{(\kappa)}, \mathbf{t}^{(\kappa)})$*. Consequently, once initialized from a feasible point* $(\mathbf{V}^{(0)}, \mathbf{t}^{(0)})$ *to (24), the* κ*-th QP iteration (41) generates a sequence* $\{\mathbf{V}^{(\kappa)}\}$ *of feasible and improved points toward the nonconvex program (24), which converges to an optimal solution of (15). Under the stopping criterion*

$$\left| \left(\mathcal{P}(\mathbf{V}^{(\kappa+1)}, \mathbf{t}^{(\kappa+1)}) - \mathcal{P}(\mathbf{V}^{(\kappa)}, \mathbf{t}^{(\kappa)}) \right) / \mathcal{P}(\mathbf{V}^{(\kappa)}, \mathbf{t}^{(\kappa)}) \right| \leq \epsilon \tag{43}$$

for a given tolerance $\epsilon > 0$*, the QP iterations will terminate after finitely many iterations.*

Proof The proof of the above proposition is based on the theory of sequential optimization [40]. For completeness, it is provided in the Appendix section. □

The proposed path-following quadratic prgramming that solves problem (15) is summarized in Algorithm 1.

Algorithm 1 Path-following quadratic programming for EE optimization.

Initialization: Set $\kappa := 0$, and choose a feasible point $(\mathbf{V}^{(0)}, \mathbf{t}^{(0)})$ to (24).

κ-th iteration: Solve (41) for an optimal solution $(\mathbf{V}^*, \mathbf{t}^*)$ and set $\kappa := \kappa + 1$, $(\mathbf{V}^{(\kappa)}, \mathbf{t}^{(\kappa)}) := (\mathbf{V}^*, \mathbf{t}^*)$ and calculate $\mathcal{P}(\mathbf{V}^{(\kappa)}, \mathbf{t}^{(\kappa)})$. Stop if $\left| \left(\mathcal{P}(\mathbf{V}^{(\kappa)}, \mathbf{t}^{(\kappa)}) - \mathcal{P}(\mathbf{V}^{(\kappa-1)}, \mathbf{t}^{(\kappa-1)}) \right) / \mathcal{P}(\mathbf{V}^{(\kappa-1)}, \mathbf{t}^{(\kappa-1)}) \right| \leq \epsilon$.

Before closing this section, it is pointed out that a feasible initial point $(\mathbf{V}^{(0)}, \mathbf{t}^{(0)})$ to (24) can be founded by solving

$$\max_{\mathsf{V}} \min_{(i,j_{\mathsf{D}})\in\mathcal{S}_1} \left\{ \frac{f_{i,j_{\mathsf{D}}}(\mathsf{V})}{r_{i,j_{\mathsf{D}}}^{\min}}, \frac{f_i(\mathsf{V})}{r_i^{\mathsf{U},\min}} \right\} : (15b), (15c), \tag{44}$$

with iterations

$$\max_{\mathsf{V}} \min_{(i,j_{\mathsf{D}})\in\mathcal{S}_1} \left\{ \frac{\Theta_{i,j_{\mathsf{D}}}^{(\kappa)}(\mathsf{V})}{r_{i,j_{\mathsf{D}}}^{\min}}, \frac{\Theta_i^{(\kappa)}(\mathsf{V})}{r_i^{\mathsf{U},\min}} \right\} : (15b), (15c), \tag{45}$$

which terminate as soon as

$$f_{i,j_{\mathsf{D}}}(\mathbf{V}^{(\kappa)})/r_{i,j_{\mathsf{D}}}^{\min} \geq 1 \text{ and } f_i(\mathbf{V}^{(\kappa)})/r_i^{\mathsf{U},\min} \geq 1, \ \forall (i,j_{\mathsf{D}}) \in \mathcal{S}_1. \tag{46}$$

4 Numerical results

For the purpose of illustrating the performance advantage (in terms of the EE) of the proposed FD precoder design, the FD BSs can be reconfigured to operate in the HD mode with $N = N_1 + N_2$ antennas at each BS. In particular, each BS operating in the HD mode serves all the DLUs in the downlink and all the ULUs in the uplink, albeit in two separate resource blocks (e.g., time or frequency). We then apply Algorithm 1 to solve the EE optimization problems (16) and (18). Suppose that $\mathbf{V}^{\text{opt,DL}}$ and $\mathbf{V}^{\text{opt,UL}}$ are their optimal solutions. Accordingly, we compare the optimal value of (15) with

$$\min_{i\in\mathcal{I}} \frac{\left(\sum_{j_{\mathsf{D}}\in\mathcal{D}} f_{i,j_{\mathsf{D}}}(\mathbf{V}^{\text{opt,DL}}) + f_i^{\text{UL}}(\mathbf{V}^{\text{opt,UL}}) \right)/2}{\zeta \left(\sum_{j_{\mathsf{D}}\in\mathcal{D}} ||\mathbf{V}_{i,j_{\mathsf{D}}}^{\text{opt}}||^2 + \sum_{j_{\mathsf{U}}\in\mathcal{U}} ||\mathbf{V}_{i,\ell_{\mathsf{U}}}^{\text{opt}}||^2 \right) + P^{\text{BS}} + UP^{\text{UE}}}, \tag{47}$$

Table 1 Simulation parameters used in all numerical examples

Parameter	Value
Carrier frequency	2 GHz
System bandwidth	10 MHz
Maximum BS transmit power, $P_{\mathrm{BS}}^{\max}$	20 W
Maximum user transmit power, $P_{\mathrm{UE}}^{\max}$	150 mW
Noise power density	−174 dBm/Hz
Noise figure at a DLU receiver	9 dB
Noise figure at a BS receiver	5 dB

where the fraction 1/2 in the numerator accounts for the fact that two time slots are used in HD downlink and uplink communications and $P^{\mathrm{BS}} = (N_1 + N_2)P_b$.

The channel matrix between a BS and a user at a distance d is generated according to the path loss model for line-of-sight (LOS) communications as $10^{-PL_{\mathrm{LOS}}/20}\tilde{H}$, where $PL_{\mathrm{LOS}} = 103.8 + 20.9\log_{10} d$ and each entry of $\tilde{H}$ is an independent circularly symmetric Gaussian random variable with zero mean and unit variance [41]. The channel matrix from a ULU to a DLU at a distance d is assumed to follow the non-line-of-sight (NLOS) path loss model as $10^{-PL_{\mathrm{NLOS}}/20}\tilde{H}$ with $PL_{\mathrm{NLOS}} = 145.4 + 37.5\log_{10} d$ [41].

For the FD mode, the number N_1 of transmit antennas and the number N_2 of receive antennas at a BS are 4 and 2, respectively. The numbers of concurrent downlink and uplink data streams are assumed to be equal to the number of antennas at a DLU/ULU, i.e., $d_1 = d_2 = N_r$. The precoding matrices $\mathsf{V}_{i,j_{\mathrm{D}}}$ and $\mathsf{V}_{i,j_{\mathrm{U}}}$ in (2) and (7) are of dimensions $N_1 \times N_r$ and $N_r \times N_r$, respectively. The rate constraints in (15d) and (15e) are set as $r_{i,j_{\mathrm{D}}}^{\min} = 2$ bps/Hz and $r_i^{\mathrm{U,min}} = 2$ bps/Hz, respectively. The circuit powers for each antenna in BS and UE are $P_b = 1.667$ W and $P_u = 50$ mW, respectively [37]. To arrive at the final figures, 100 simulation runs are carried out and the results are averaged. Table 1 lists other 3GPP LTE network parameters that are used in all simulations [41]. For simplicity, the drain efficiency of power amplifier ζ is assumed to be 100% for both the downlink and uplink transmissions.

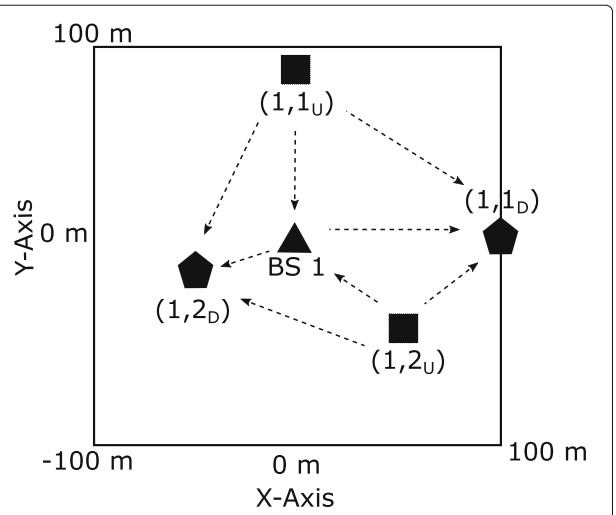

Fig. 2 A single-cell network with 2 DLUs and 2 ULUs

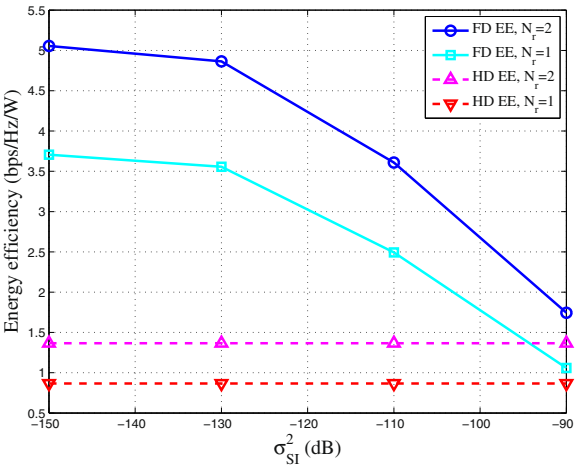

Fig. 3 Energy efficiency of the single-cell network for FD and HD modes

4.1 Effect of SI in a single-cell network with fixed users

The example network in Fig. 2 is used to study the energy efficiency performance of Algorithm 1. By considering a single-cell network with fixed-location users, one can focus on the effect of SI while isolating those of the intracell and intercell interferences. Figure 3 shows the energy efficiency results for two cases of $N_r = 1$ and $N_r = 2$.

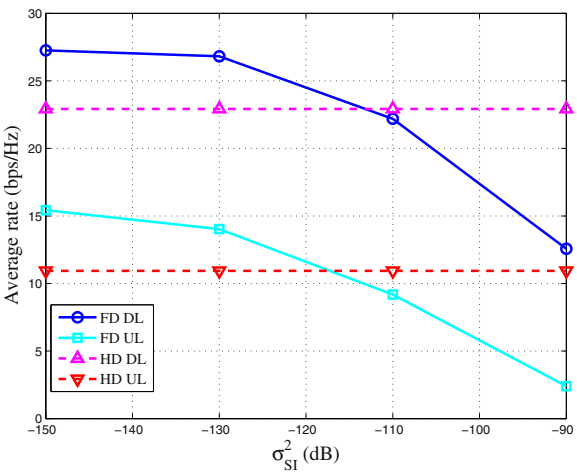

Fig. 4 Data rates of DL and UL for FD and HD modes with $N_r = 2$ in the single-cell network

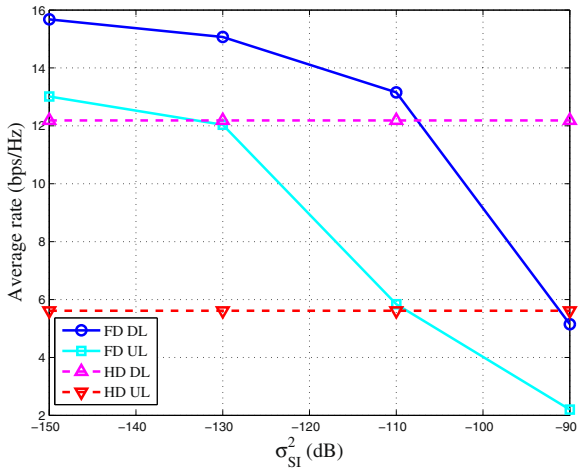

Fig. 5 Data rates of DL and UL for FD and HD modes with $N_r = 1$ in the single-cell network

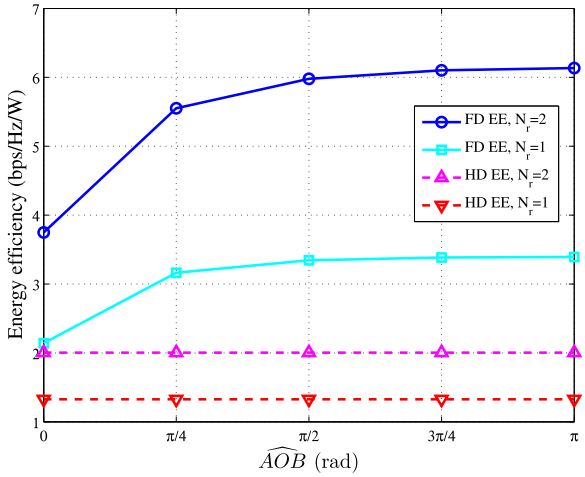

Fig. 7 Energy efficiency of the single-cell network under FD and HD modes

It is clear that the EE under the FD mode degrades as σ^2_{SI} increases. In particular, FD EE is more than double the HD EE when $\sigma^2_{SI} \leq -100$ dB. Figures 4 and 5 further illustrate the data rates of FD and HD modes for $N_r = 2$ and $N_r = 1$, respectively. It can be seen that, due to the adverse effect of SI, the data rates of DL and UL in the FD model degrade with increasing of σ^2_{SI}. For the case of $N_r = 2$, Fig. 4 shows that the data rates in the FD mode are higher than that of the HD mode when $\sigma^2_{SI} \leq -120$ dB. Similarly, it is clear from Fig. 5 that the data rates in the FD mode with $N_r = 1$ are superior than that in the HD mode when $\sigma^2_{SI} \leq -110$ dB.

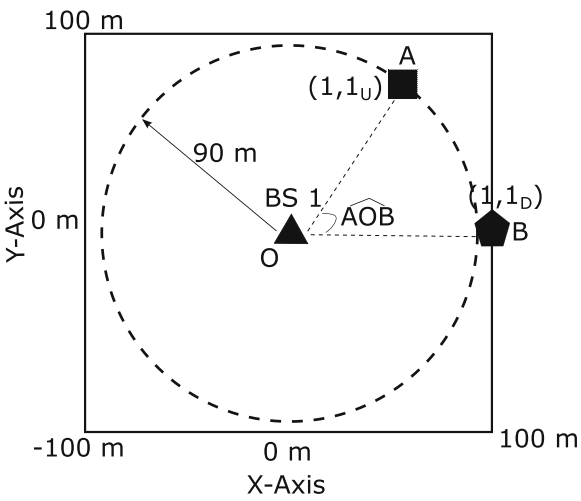

Fig. 6 *A* single-cell network with one fixed DLU and one moving ULU. The DLU location is fixed at point *B*, whereas the ULU is located at any point A on the circle of radius of 90 m

4.2 Effect of intracell interference in a single-cell network

The example network in Fig. 6 is examined to study the EE performance of Algorithm 1 when the intracell interference changes but σ^2_{SI} is fixed at $\sigma^2_{SI} = -110$ dB. The location of the DLU is fixed at point B but the location of the ULU is varied. For each position of the ULU at a point A on a circle of radius 90 m, the EE quantity is found by Algorithm 1. By keeping the small-scale fading parameter unchanged, a small angle $\widehat{AOB}$ in Fig. 6 results in a small path loss and accordingly a large intracell interference level.

It can be observed from Fig. 7 that the FD EE is always much higher than the HD EE if the intracell interference is sufficiently small. The largest gain in EE is achieved when

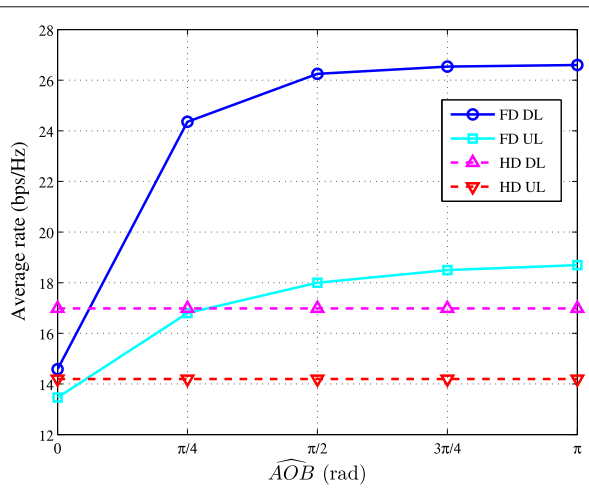

Fig. 8 Data rates of DL and UL for FD and HD modes with $N_r = 2$ in the single-cell network

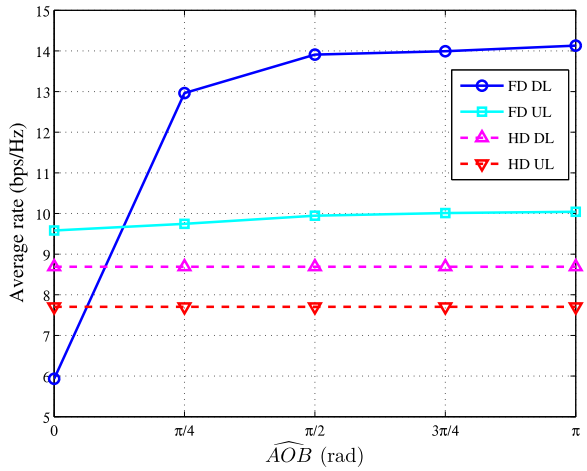

Fig. 9 Data rates of DL and UL for FD and HD modes with $N_r = 1$ in the single-cell network

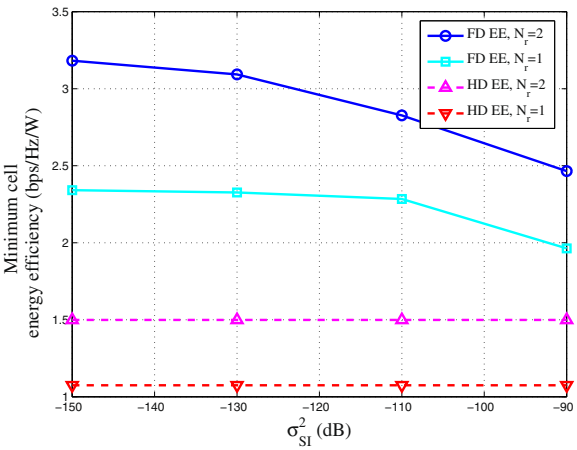

Fig. 11 Effect of SI on the energy efficiency in a three-cell network

the ULU-DLU distance is maximum (i.e., $\widehat{\text{AOB}} = \pi$), in which case, the intracell interference is smallest. In addition, Figs. 8 and 9 plot the data rates of FD and HD modes for $N_r = 2$ and $N_r = 1$, respectively. For the case of $N_r = 2$, the data rates of FD DL at $\widehat{\text{AOB}} = 0$ are smaller than that of the HD DL. This is expected since when the ULU is very close to DLU at $\widehat{\text{AOB}} = 0$, the intracell interference is strongest. When the ULU-DLU distance becomes larger, the data rates of FD are significantly higher than the data rates of HD. In the case of $N_r = 1$, the data rates of FD DL are only smaller than that of HD DL at $\widehat{\text{AOB}} = 0$, while the data rates of FD UL are higher than that of HD UL at every position of the ULU.

4.3 Multi-cell networks

In the last simulation scenario, we compare the FD EE and HD EE for a three-cell network as depicted by Fig. 10. The positions of the ULU and DLU in each cell are fixed at distances $2r/3 = 66.67$ m and $r/2 = 50$ m from their serving BS, respectively. Figure 11 shows that the EE decreases with the increasing level of SI.

The convergence behavior of Algorithm 1 is demonstrated in Fig. 12 for the network in Fig. 10, where the error tolerance for convergence is set as $\epsilon = 10^{-3}$. As can be seen, the proposed algorithm monotonically improves the objective value after every iteration. Table 2 shows that

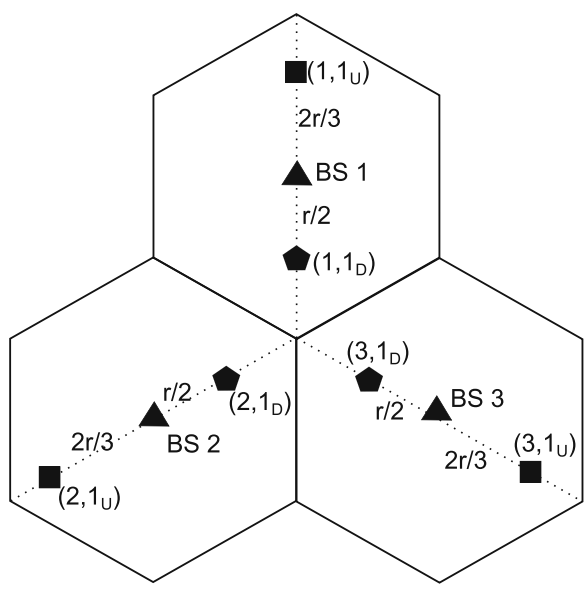

Fig. 10 A three-cell network with 1 DLU and 1 ULU. The cell radius is $r = 100$ m

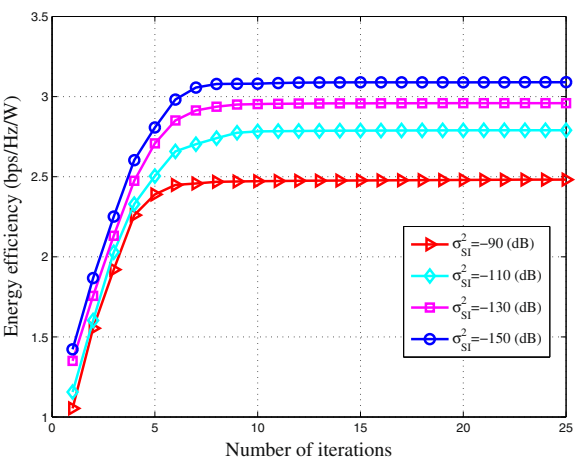

Fig. 12 Convergence of Algorithm 1 for the FD energy efficiency with $\epsilon = 10^{-3}$

Table 2 The average number of iterations required by Algorithm 1

σ_{SI}^2 (dB)	-150	-130	-110	-90
Average number of iterations	32.4	20.3	25.7	18.5

the convergence occurs within about 32 iterations. Note also that each iteration only involves one simple convex QP, which can be solved very efficiently by any available convex solvers such as CVX [42]. The data rates of the minimum cell energy efficiency for $N_r = 2$ and $N_r = 1$ are provided in Figs. 13 and 14, respectively. For the case of $N_r = 2$, the data rates of FD DL are slightly smaller than that of HD DL, but the gap between FD UL and HD UL data rates becomes larger as σ_{SI}^2 increases. In the case of $N_r = 1$, although the data rates of FD DL are higher than that of the HD DL, it decreases with increasing σ_{SI}^2. On the contrary, the data rates of FD UL are smaller than that of the HD UL.

5 Conclusions

We have designed novel linear precoders for base stations and users in order to maximize the energy efficiency of a multicell network in which full-duplex BSs simultaneously transmit to and receive from their half-duplex users. The precoders are found by a low-complexity iterative algorithm that requires solving only one simple convex quadratic program at each iteration. It has also been proved that the proposed path-following algorithm is guaranteed to monotonically converge. Simulation results have been presented in various network scenarios to demonstrate the performance advantage of the proposed precoders in terms of energy efficiency.

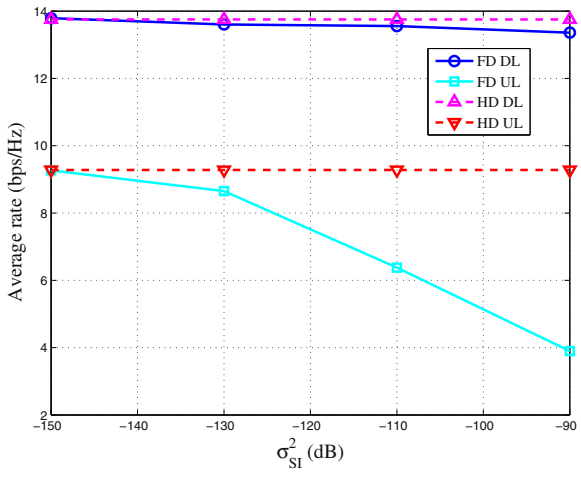

Fig. 13 Data rates of DL and UL for FD and HD modes with $N_r = 2$ in a three-cell network

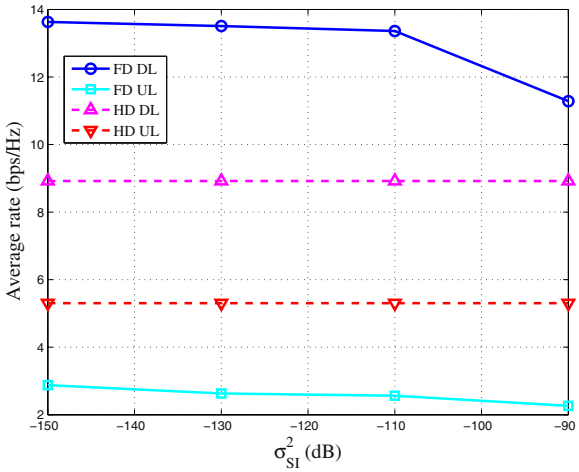

Fig. 14 Data rates of DL and UL for FD and HD modes with $N_r = 1$ in a three-cell network

Endnotes

[1] Function $\ln|\mathbf{I} + \mathsf{X}|$ is concave in $\mathsf{X} \succeq 0$ so its first-order approximation at $\mathbf{0}$, which is Trace(X), is its upper bound [38].

[2] Function x^2/t is convex on $\mathsf{x} > 0$ and $\mathsf{t} > 0$, so its first-order approximation at $(\bar{x}, \bar{t})$, which is $2\bar{x}\mathsf{x}/\bar{t} - \bar{x}\mathsf{t}/\bar{t}^2$, is its lower bound [38].

Appendix

Proof of Proposition 1

By (31) and (32), any (V, t) feasible to the convex program (41) is also feasible to the nonconvex program (24). As $(\mathbf{V}^{(\kappa)}, \mathbf{t}^{(\kappa)})$ is feasible to (41), it follows that

$$\begin{aligned}\mathcal{P}(\mathbf{V}^{(\kappa+1)}, \mathbf{t}^{(\kappa+1)}) &\geq \mathcal{P}^{(\kappa)}(\mathbf{V}^{(\kappa+1)}, \mathbf{t}^{(\kappa+1)}) \\ &> \mathcal{P}^{(\kappa)}(\mathbf{V}^{(\kappa)}, \mathbf{t}^{(\kappa)}) = \mathcal{P}(\mathbf{V}^{(\kappa)}, \mathbf{t}^{(\kappa)})\end{aligned} \tag{48}$$

as far as $(\mathbf{V}^{(\kappa+1)}, \mathbf{t}^{(\kappa+1)}) \neq (\mathbf{V}^{(\kappa)}, \mathbf{t}^{(\kappa)})$, hence showing (42).

Since the sequence $\{(\mathbf{V}^{(\kappa)}, \mathbf{t}^{(\kappa)})\}$ is bounded by constraint (15c), by Cauchy's theorem, there is a convergent subsequence $\{(\mathbf{V}^{(\kappa_\nu)}, \mathbf{t}^{(\kappa_\nu)})\}$, i.e.,

$$\lim_{\nu \to +\infty} \left[\mathcal{P}(\mathbf{V}^{(\kappa_{\nu+1})}, \mathbf{t}^{(\kappa_{\nu+1})}) - \mathcal{P}(\mathbf{V}^{(\kappa_\nu)}, \mathbf{t}^{(\kappa_\nu)})\right] = 0. \tag{49}$$

For every κ, there is ν such that $\kappa_\nu \leq \kappa$ and $\kappa + 1 \leq \kappa_{\nu+1}$. It follows from (42) that

$$\begin{aligned}0 &\leq \lim_{\kappa \to +\infty} \left[\mathcal{P}(\mathbf{V}^{(\kappa+1)}, \mathbf{t}^{(\kappa+1)}) - \mathcal{P}(\mathbf{V}^{(\kappa)}, \mathbf{t}^{(\kappa)})\right] \\ &\leq \lim_{\nu \to +\infty} \left[\mathcal{P}(\mathbf{V}^{(\kappa_{\nu+1})}, \mathbf{t}^{(\kappa+1)}) - \mathcal{P}(\mathbf{V}^{(\kappa_\nu)}, \mathbf{t}^{(\kappa_\nu)})\right] \\ &= 0,\end{aligned} \tag{50}$$

showing

$$\lim_{\kappa \to +\infty} \left[\mathcal{P}(\mathbf{V}^{(\kappa+1)}, \mathbf{t}^{(\kappa+1)}) - \mathcal{P}(\mathbf{V}^{(\kappa)}, \mathbf{t}^{(\kappa)})\right] = 0. \tag{51}$$

For a given tolerance $\epsilon > 0$, the iterations will therefore terminate after finitely many iterations under the stopping criterion

$$\left|\left(\mathcal{P}_1(\mathbf{V}^{(\kappa+1)}, \mathbf{t}^{(\kappa+1)}) - \mathcal{P}(\mathbf{V}^{(\kappa)}, \mathbf{t}^{(\kappa)})\right) / \mathcal{P}(\mathbf{V}^{(\kappa)}, \mathbf{t}^{(\kappa)})\right| \leq \epsilon. \tag{52}$$

Each accumulation point $(\bar{\mathbf{V}}, \bar{\mathbf{t}})$ of the sequence $\{(\mathbf{V}^{(\kappa)}, \mathbf{t}^{(\kappa)})\}$ satisfies the minimum principle necessary condition for optimality [40].

Acknowledgements
The work is supported by NSF of China (61271213, 61673253) and the Ph.D. Programs Foundation of Ministry of Education of China (20133108110014).

Competing interests
The authors declare that they have no competing interests.

Author details
[1]School of Communication and Information Engineering, Shanghai University, Shanghai, China. [2]Faculty of Engineering and Information Technology, University of Technology Sydney, Broadway, NSW 2007, Sydney, Australia. [3]Department of Electrical and Computer Engineering, University of Saskatchewan, Saskatoon, Canada.

Received: 2 July 2016 Accepted: 23 February 2017
Published online: 14 March 2017

References

1. A Fehske, G Fettweis, J Malmodin, G Biczok, The global footprint of mobile communications: the ecological and economic perspective. IEEE Commun. Mag. **49**(8), 55–62 (2011)
2. G Auer, et al., How much energy is needed to run a wireless network?. IEEE Wireless Cmmun. Mag. **18**, 5 (2011)
3. Y Chen, S Zhang, S Xu, G Li, Fundamental trade-offs on green wireless networks. IEEE Commun. Mag. **49**(6), 30–37 (2011)
4. Z Hasan, H Boostanimehr, VK Bhargava, Green cellular networks: a survey, some research issues and challenges. IEEE Commun. Surv. Tutorials. **13**(4), 524–540 (2011)
5. YS Soh, TQS Quek, M Kountouris, H Shin, Energy efficient heterogeneous cellular networks. IEEE J. Sel. Areas Commun. **31**(5) (2013)
6. Z Xu, C Yang, GY Li, Y Liu, S Xu, Energy-efficient CoMP precoding in heterogeneous networks. IEEE Trans. Signal Process. **62**(4), 1005–1017 (2014)
7. E Bjornson, L Sanguinetti, J Hoydis, M Debbah, Optimal design of enerygy-efficient multi-user MIMO systems: is massive MIMO the answer. IEEE Trans. Wireless Commun. **14**(6), 3059–3075 (2015)
8. Y Xin, D Wang, J Li, H Zhu, J Wang, X You, Area spectral efficiency and area energy efficiency of massive MIMO cellular systems. IEEE Trans. Vehic. Technol. **65**(5), 3243–3254 (2016)
9. RLG Cavalcante, S Stanczak, M Schubert, A Eisenlatter, U Turke, Toward energy-efficienct 5G wireless communications technologies. IEEE Sig. Process. Mag. **13**(11), 24–34 (2014)
10. I C-L, C Rowell, S Han, Z Xu, G Li, Z Pan, Toward green and soft: a 5G perspective. IEEE Commun. Mag. **13**(2), 66–73 (2014)
11. S Buzzi, I C-L, TE Klein, HV Poor, C Yang, A Zappone, A survey of energy-efficient techniques for 5G networks and challenges ahead. IEEE J. Sel. Areas Commun. **34**(4), 697–709 (2016)
12. CTK Ng, H Huang, Linear precoding in cooperative MIMO cellular networks with limited coordination clusters. IEEE J. Sel. Areas Commun. **28**(9), 1446–1454 (2010)
13. SS Christensen, R Agarwal, E Carvalho, JM Cioffi, Weighted sum-rate maximization using weighted MMSE for MIMO-BC beamforming design. IEEE Trans. Wirel. Commun. **7**(12), 4792–4799 (2008)
14. K Wang, X Wang, W Xu, X Zhang, Coordinated linear precoding in downlink multicell MIMO-OFDMA networks. IEEE Trans. Sig. Process. **60**(8), 4264–4277 (2012)
15. B Song, RL Cruz, BD Rao, Network duality for multiuser MIMO beamforming networks and applications. IEEE Trans. Commun. **55**(3), 618–630 (2007)
16. DWH Cai, TQS Quek, CW Tan, SH Low, Max-min SINR coordinated multipoint downlink transmission - Duality and algorithms. IEEE Trans. Sig. Process. **60**(10), 5384–5395 (2012)
17. Y Huang, CW Tan, BD Rao, Joint beamforming and power control in coordinated multicell: max-min duality, effective network and large system transition. IEEE Trans. Wirel. Commun. **12**(6), 2730–2742 (2013)
18. Y-S Choi, H Shirani-Mehr, Simultaneous transmission and reception: algorithm, design and system level performance. IEEE Trans. Wirel. Commun. **12**(12), 5992–6010 (2013)
19. A Sabharwal, et al., In-band full-duplex wireless: challenges and opportunities. IEEE J. Sel. Areas Commun. **32**(9), 1637–1652 (2014)
20. M Heino, et al., Recent advances in antenna design and interference cancellation algorithms for in-band full duplex relays. IEEE Commun. Mag. **5**, 91–101 (2015)
21. E Everett, A Sahai, A Sabharwal, Passive self-interference suppression for full-duplex infrastructure nodes. IEEE Trans. Wirel. Commun. **13**(2), 680–694 (2014)
22. M Duarte, A Sabharwal, V Aggarwal, R Jana, KK Ramakrishnan, CW Rice, NK Shankaranarayanan, Design and characterization of a full-duplex multiantenna system for WiFi networks. IEEE Trans. Veh. Technol. **63**(3), 1160–1177 (2014)
23. L Anttila, et al., in *Modeling and efficient cancelation of nonlinear self-interference in MIMO full-duplex transceivers*. Proc. of Globecom (IEEE, Austin, 2014), pp. 777–783
24. HHM Tam, HD Tuan, DT Ngo, Successive convex quadratic programming for quality-of-service management in full-duplex MU-MIMO multicell networks. IEEE Trans. Comm. **64** (2016)
25. W Dinkelbach, On nonlinear fractional programming. Manag. Sci. **13**(7), 492–498 (1967)
26. DWK Ng, ES Lo, R Schober, Energy-efficient resource allocation in multi-cell OFDMA systems with limited feedback capacity. IEEE Trans. Wirel. Commun. **11**(10), 3618–3631 (2012)
27. A Zappone, E Jorswieck, Energy efficiency in wireless networks via fractional programming theory. Found Trends Comm Inf Theory. **11**(3-4), 185–396 (2015)
28. A Zappone, L Sanguinetti, G Bacci, E Jorswieck, M Debbah, Energy-efficient power control: a look at 5G wireless technologies. IEEE Trans. Sig. Process. **64**(4), 1668–1683 (2016)
29. O Tervo, LN Tran, M Juntti, Optimal energy-efficient transmit beamforming for multi-user MISO downlink. IEEE Trans. Sig. Process. **63**(10), 5574–5588 (2015)
30. QD Vu, LN Tran, R Farrell, EK Hong, Energy-efficient zero-forcing precoding design for small-cell networks. IEEE Trans. Commun. **64**(2), 790–804 (2016)
31. H Weingarten, Y Steinberg, S Shamai, The capacity region of the Gaussian multiple-input multiple-output broadcast channel. IEEE Trans. Inf. Theory. **52**(9), 3936–3964 (2006)
32. L-N Tran, M Juntti, M Bengtsson, B Ottersten, Weighted sum rate maximization for MIMO broadcast channels using dirty paper coding and zero-forcing methods. IEEE Trans. Commun. **61**(6), 2362–2372 (2013)
33. W Yu, JM Cioffi, Sum capacity of Gaussian vector broadcast channels. IEEE Trans. Inf. Theory. **50**(9), 1875–1892 (2004)
34. M Duarte, C Dick, A Sabharwal, Experiment-driven characterization of full-duplex wireless systems. IEEE Trans. Wirel. Commun. **11**(12), 4296–4307 (2012)
35. D Korpi, et al., Full-duplex transceiver system calculations: analysis of adc and linearity challenges. IEEE Trans. Wirel. Commun. **13**(7), 3821–3836 (2014)
36. D Tse, P Viswanath, *Fundamentals of wireless communication*. (Cambridge University Press, New York, 2005)
37. C Xiong, GY Li, S Zhang, Y Chen, S Xu, Energy-efficient resource allocation in OFDMA networks. IEEE Trans. Commun. **60**(12), 3767–3778 (2012)
38. H Tuy, *Convex analysis and global optimization (second Edition)*. (Springer, Verlag Berlin Heidelberg, 2016)
39. B Dacorogna, P Marechal, The role of perspective functions in convexity, polyconvexity, rank-one convexity and separate convexity. J. Convex Anal. **15**(2), 271–284 (2008)

40. BR Marks, GP Wright, A general inner approximation algorithm for nonconvex mathematical programms. Oper. Res. **26**(4), 681–683 (1978)
41. 3GPP TS 36.814 V9.0.0, 3GPP technical specification group radio access network, evolved universal terrestrial radio access (E-UTRA): Further advancements for E-UTRA physical layer aspects (Release 9) (2010)
42. M Grant, S Boyd, CVX: Matlab software for disciplined convex programming, version 2.1 (2014). http://cvxr.com/cvx. Accessed 1 May 2016.